

An *XMM-Newton* observation of Ton S180: Constraints on the continuum emission in ultrasoft Seyfert galaxies

S. Vaughan,¹ Th. Boller,² A. C. Fabian,¹ D. R. Ballantyne,¹ W. N. Brandt³ and J. Trümper²

¹*Institute of Astronomy, Madingley Road, Cambridge CB3 0HA*

²*Max-Planck-Institut für extraterrestrische Physik, Postfach 1603, 85748 Garching, Germany*

³*Department of Astronomy and Astrophysics, Pennsylvania State University, 525 Davey Lab, University Park, PA 16802, USA*

Accepted 2002 July 25; Submitted 2002 July 23; in original form 2002 June 12

ABSTRACT

We present an *XMM-Newton* observation of the bright, narrow-line, ultrasoft Seyfert 1 galaxy Ton S180. The 0.3–10 keV X-ray spectrum is steep and curved, showing a steep slope above 2.5 keV ($\Gamma \sim 2.3$) and a smooth, featureless excess of emission at lower energies. The spectrum can be adequately parameterised using a simple double power-law model. The source is strongly variable over the course of the observation but shows only weak spectral variability, with the fractional variability amplitude remaining approximately constant over more than a decade in energy. The curved continuum shape and weak spectral variability are discussed in terms of various physical models for the soft X-ray excess emission, including reflection off the surface of an ionised accretion disc, inverse-Compton scattering of soft disc photons by thermal electrons, and Comptonisation by electrons with a hybrid thermal/non-thermal distribution. We emphasise the possibility that the strong soft excess may be produced by dissipation of accretion energy in the hot, upper atmosphere of the putative accretion disc.

Key words: galaxies: active – galaxies: Seyfert: general – galaxies: individual: Ton S180 – X-ray: galaxies

1 INTRODUCTION

Many Seyfert 1 galaxies and radio-quiet quasars possess X-ray spectra that steepen below ~ 2 keV. This ‘soft excess’ emission, usually defined as the excess emission over and above the hard X-ray power-law, was first seen in spectra obtained by *HEAO-1* A2 (Pravdo et al. 1981), *EXOSAT* (Arnaud et al. 1985; Turner & Pounds 1989) and *Einstein* (Bechtold et al. 1987). Its physical origin remains uncertain, as does its connection with the so-called ‘big blue bump’ emission rising through the ultraviolet, although it is often associated with thermal emission from the putative accretion disc (e.g. Arnaud et al. 1985; Czerny & Elvis 1987).

Boller, Brandt & Fink (1996) and Laor et al. (1997) showed that the objects with the steepest soft X-ray spectra (implying the strongest soft excesses) tend to have relatively narrow optical $H\beta$ lines; many are classified optically as narrow-line Seyfert 1s (NLS1s; Osterbrock & Pogge 1985). These ‘ultrasoft’ Seyferts often show other notable properties such as very rapid X-ray variability (e.g. Forster & Halpern 1996; Boller et al. 1997; Turner et al. 1999; Leighly 1999a; Brandt et al. 1999) and strong optical Fe II emission (e.g. Lawrence et al. 1997; Vaughan et al. 2001). The X-ray spectral form, X-ray variability and optical broad-line properties seem interconnected.

Here we report the results of a 30 ksec *XMM-Newton* observation of Tonantzintla S180 ($z = 0.062$) obtained as part of a guaranteed time programme (PI: Th. Boller) to study the timing and spec-

tral properties of ultrasoft NLS1s using *XMM-Newton*. Ton S180 is one of the X-ray brightest ultrasoft Seyferts (Vaughan et al. 1999; Leighly 1999a) and its luminosity is such that it is often classified as a quasar. Previous X-ray observations with *ASCA* (Turner, George & Nandra 1998; Vaughan et al. 1999; Leighly 1999b; Ballantyne, Iwasawa & Fabian 2001) and *BeppoSAX* (Comastri et al. 1998) showed a strong excess of soft emission and tentative evidence for an ionised iron line. The more recent high-resolution *Chandra* LETGS spectrum (Turner et al. 2001b) showed no strong, narrow absorption or emission features and showed the soft X-ray continuum is smooth and featureless.

The rest of the paper is organised as follows. In the following section the observation and basic data reduction procedures are outlined. Section 3 describes the X-ray spectral fitting results. This is followed by an analysis of the variability properties of Ton S180 in section 4. The implications of these results are discussed in section 5.

2 OBSERVATION AND DATA REDUCTION

XMM-Newton (Jansen et al. 2001) carries three European Photon Imaging Cameras (EPIC), specifically two MOS (Turner et al. 2001a) and one pn (Strüder et al. 2001) CCD camera. In addition

there are two Reflection Grating Spectrometers (RGS; den Herder et al. 2001) and an Optical Monitor (OM; Mason et al. 2001).

XMM-Newton observed Ton S180 on 2000 December 14 (revolution 0186) for a duration of ~ 30 ksec, during which all instruments were operating nominally. The MOS1 camera was in timing mode, which severely complicates the analysis, and these data are ignored in the present paper. Both the MOS2 and pn were operated in small window mode to reduce “pile up” from this relatively bright (few ct s^{-1}) source, and all EPIC cameras used the medium filter. The RGS was operated in standard (Spectro+Q) mode. Extraction of science products from the Observation Data Files (ODFs) followed standard procedures using the *XMM-Newton* Science Analysis System v5.3 (SAS).

The raw data were processed to produce calibrated event lists and screened to remove unwanted hot, dead or flickering pixels, and events due to electronic noise. Light curves extracted from these event lists showed the background to be stable throughout the duration of the observation. The total amount of “good” exposure time selected was 28, 644 s and 20, 338 s for MOS2 and pn, respectively, and 30, 232 s and 29, 321 s for RGS1 and RGS2. (The lower pn exposure is due to the lower “live time” of the pn camera in small-window mode, ~ 71 per cent; Strüder et al. 2001).

Source data were extracted from circular regions of radius $35''$ from the MOS2 and pn, and show no signs of pile-up. Background events were extracted from off-source regions. Events corresponding to patterns 0–12 (single–quadruple pixel events) were extracted from MOS2 and patterns 0–4 (singles and doubles) were used for the pn analysis, after checking for consistency with the data extracted using only single pixel events (pattern 0). Standard redistribution matrices (m2_r6_a11_15.rmf for MOS2 and epn_sw20_sdY9.rmf for the pn) were used, and ancillary response files were generated using ARFGEN V1.48.8. First-order RGS spectra were extracted using the RGSPROC V1.3.3 script, and appropriate response matrices were generated using RGSRMFGEN V1.44.5. The total number of “good” source events extracted was 2.9×10^5 for the pn, 8.8×10^4 for MOS2 and 1.4×10^4 for each RGS.

3 SPECTRAL ANALYSIS

The source spectra were grouped such that each spectral bin contains at least 20 counts, and they were fitted using the XSPEC V11.1 software package (Arnaud 1996). The quoted errors on the derived best-fitting model parameters correspond to a 90 per cent confidence level for one interesting parameter (i.e., a $\Delta\chi^2 = 2.7$ criterion) unless otherwise stated. Values of $H_0 = 70 \text{ km s}^{-1} \text{ Mpc}^{-1}$ and $q_0 = 0.5$ are assumed throughout the paper, and fit parameters are quoted for the rest frame of the source.

3.1 The 2.5–10 keV spectral form

The two EPIC spectra were first examined separately to test for discrepancies. The data were fitted over 2.5–10 keV using a model comprised of a power-law modified by Galactic absorption (with fixed column density $N_H = 1.55 \times 10^{20} \text{ cm}^{-2}$; Dickey & Lockman 1990). This provided a reasonable fit to both spectra ($\chi^2 = 115.0/153$ degrees of freedom and $\chi^2 = 339.8/336$ dof for the MOS2 and pn data, respectively) with consistent normalisations and photon indices ($\Gamma = 2.29 \pm 0.10$ for MOS2 and $\Gamma = 2.25 \pm 0.06$ for pn).

Given this good agreement between the two spectra over the

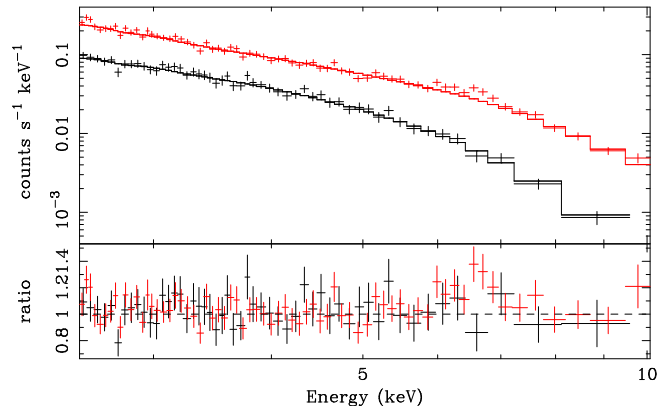


Figure 1. EPIC pn (upper data) and MOS2 spectra in the 2.5–10 keV range compared to a simple power-law model (the energies have been shifted into the source frame). The upper panel shows the count spectra (crosses) and the power-law model folded through the detector responses (histograms). The lower panel shows the fit residuals.

2.5–10 keV energy range, the data were fitted simultaneously in the rest of the spectral analysis, but in each fit the residuals from the two spectra were examined separately to check for inconsistencies. The relative normalisations were left free to allow for slight differences in absolute flux calibration between the two detectors. Figure 1 shows the two EPIC spectra compared to a simple power-law fitted over 2.5–10 keV. As expected from the fits to the individual spectra, this model ($\Gamma = 2.26_{-0.12}^{+0.05}$) is in excellent agreement with the data ($\chi^2 = 455.1/490$ dof).

3.1.1 Iron $K\alpha$ emission

The pn spectrum shows positive residuals around ~ 7 keV which could indicate spectral features from iron K. To test for this an intrinsically narrow ($\sigma = 1$ eV) Gaussian emission line was added to the model. With the narrow line energy fixed at 6.4 keV the fit was not significantly improved; the 90 per cent upper limit of the equivalent width of a narrow, neutral iron line is $EW < 60$ eV. Allowing the line energy to be free provided an improvement to the fit ($\chi^2 = 447.3/488$ dof) but the best-fitting line energy of $E = 7.01 \pm 0.06$ keV is marginally too high for $K\alpha$ emission from even Hydrogen-like iron. The equivalent width of this line is $EW = 72 \pm 43$ eV. According to an F -test, upon adding two parameters (line flux and energy) the fit is significantly improved at 98.5 per cent confidence. Allowing the line width to be free improved the fit further ($\chi^2 = 441.5/487$ dof) with a best-fitting width of $\sigma = 0.53_{-0.33}^{+0.50}$ keV and an energy of $E = 7.01 \pm 0.31$ keV, which is consistent with $K\alpha$ emission from H-like iron. An F -test suggests the fit is improved, at 98.8 per cent confidence, upon allowing the line width to be free. This broad line is strong, with an equivalent width of $EW = 282_{-163}^{+245}$ eV. The high energy derived from the line might instead be indicating the presence of iron K absorption (at $E > 7.1$ keV), but this seems unlikely. Replacing the broad Gaussian with an absorption edge gave a worse fit ($\chi^2 = 451.8/488$ dof), with edge parameters $E = 8.33_{-0.45}^{+0.65}$ keV and $\tau = 0.15 \pm 0.14$.

Using a DISKLINE line profile (Fabian et al. 1989) to model the residuals around 7 keV provided a comparable fit to the broad Gaussian ($\chi^2 = 444.2/487$). An F -test suggests this improvement to the fit, compared to the simple power-law model, is significant at 99 per cent confidence. The best-fitting parameters of

the line were the following: rest-frame energy $E = 6.48^{+0.42}_{-0.08}$ keV, $EW = 523^{+273}_{-160}$ eV and inclination angle $i = 65^{+21}_{-9}$ deg. Allowing the other free parameters (inner radius r_{in} , outer radius r_{out} , and disc emissivity index q) to be free did not improve the fit significantly, and thus these parameters were kept fixed at $r_{in} = 6r_g$, $r_{out} = 1000r_g$ and $q = 3$. As can be seen from figure 1, the excess at ~ 7 keV in the pn data is not obvious in the MOS2 data; however, the two spectra are formally consistent with one another. When the normalisation of the DISKLINE was allowed to be free between the two detectors, the best fitting normalisations were consistent, although the normalisation from the MOS2 spectrum is poorly constrained and is consistent with zero.

The above results are suggestive of “reflection” off a (possibly ionised) accretion disc. To provide a more physically realistic description of emission from an ionised disc, the model of Ross & Fabian (1993) (see also Ballantyne et al. 2001) was fitted to the data (assuming solar abundances). The disc reflection spectrum was blurred using the LAOR kernel (Laor 1991) to simulate Doppler and gravitational effects around a black hole. The best fitting ionised disc model gives a good fit ($\chi^2 = 445.0/487$ dof) with $\Gamma = 2.43 \pm 0.13$, $R = 1.5^{+1.1}_{-0.9}$ and fairly low ionisation ($\log(\xi) < 1.9$). The LAOR profile parameters were only poorly constrained and were kept fixed (as above).

We conclude that the presence of a broad, ionised iron line (as previously suggested by Comastri et al. 1998 and Turner et al. 1998) is consistent with the XMM-Newton data, but the line parameters are only poorly constrained.

3.2 The broad-band X-ray spectrum

Having parameterised the spectrum above 2.5 keV the analysis was extended to cover the full useful spectral bandpass of XMM-Newton by including the EPIC data down to 0.3 keV and the RGS data. However, there are significant differences between the MOS2 and pn spectra below 1 keV; the difference is most pronounced around 0.56 keV. There is a similar feature present in the calibration observation of Mrk 421, which is almost certainly related to the instrumental O K-edge at 0.537 keV and seems to be most pronounced in data taken in pn small-window mode (as here). The residuals in the MOS camera are at a much lower level ($\lesssim 5$ per cent) in this spectral region. For these reasons a conservative restriction was applied to the pn data, the spectrum was fitted between 1.2–10 keV only, while the MOS2 data were used over the 0.3–10 keV band.

An extrapolation of the simple 2.5–10 keV power-law model down to 0.3 keV (Figure 2) shows a smooth upturn in the EPIC spectrum: the soft excess. There does not seem to be an obvious transition from hard power-law to soft excess in the spectrum, on the contrary, the spectrum is gently curving up to at least 2 keV.

The average observed flux in the 0.3–10 keV band was 2.2×10^{-11} erg s $^{-1}$ cm $^{-2}$ and the corresponding (unabsorbed) luminosity was $\sim 2.5 \times 10^{44}$ erg s $^{-1}$. The bolometric luminosity is most likely $\gtrsim 10^{45}$ erg s $^{-1}$ (this is a conservative estimate as Ton S180 probably harbours a strong EUV excess; Turner et al. 2002). Assuming Ton S180 is radiating at the Eddington limit (or lower) then it requires a black hole mass $M \gtrsim 10^7 M_{\odot}$ (see also Turner et al. 2001b).

3.2.1 RGS spectrum

The 0.35–1.5 keV RGS data confirm that the soft excess emission in Ton S180 is a smooth continuum, as seen by Turner et al. (2001b)

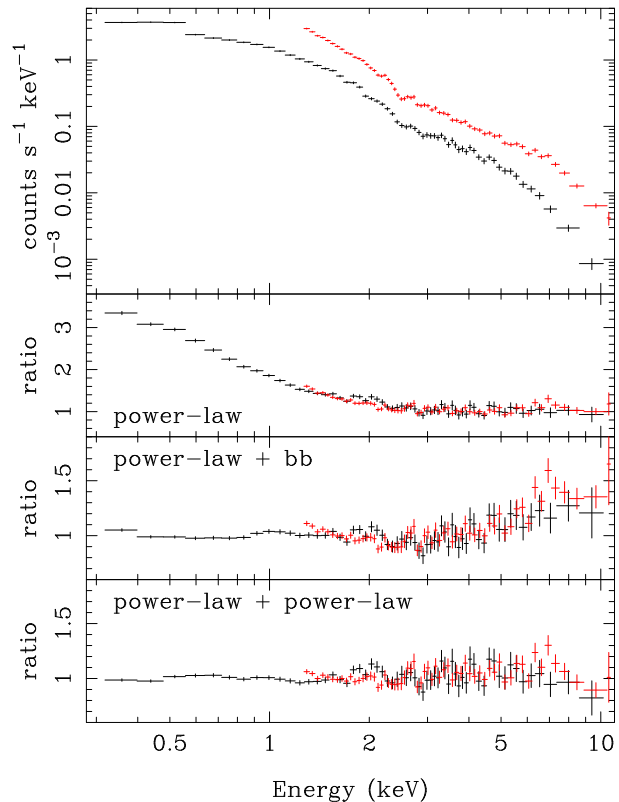


Figure 2. EPIC pn (upper data) and MOS2 spectra. The upper panel shows the count spectra, and the lower panels show the ratio of data to three different models. The second panel shows the results of fitting a single power-law model only to the data above 2.5 keV (as in figure 1) and extrapolating to lower energies, revealing the curved continuum. The bottom two panels show the results of fitting with a power-law plus blackbody or a two power-law model. (The data were rebinned for display purposes.)

from Chandra LETGS data. Figure 3 shows the background subtracted RGS spectrum of Ton S180 in flux units (RGS1 and RGS2 combined). An absorbed power-law provides a good fit to the data ($\chi^2 = 1315.2/1256$ dof) with the absorbing column fixed at the Galactic value and a power-law slope of $\Gamma = 2.77 \pm 0.03$. There are no significant sharp residuals in the RGS spectrum, the only obvious deviation from the power-law model is around 0.5–0.6 keV and is probably associated with the O K-edge in the detector response. The equivalent widths of any narrow absorption features are restricted to $EW < 1.0$ eV (90 per cent upper limit) in the 0.35–0.70 keV energy range, $EW < 1.7$ eV in the 0.7–1.0 keV range and $EW < 10$ eV in the 1.0–1.5 keV range. Thus the soft excess in Ton S180 is a smooth continuum resembling a power-law. In the following sections the EPIC spectra are used to test various physical models for the soft excess emission.

3.2.2 Phenomenological model

Given that the RGS spectrum can be fitted with a steep power law, the broad-band EPIC spectrum was first compared to a simple double power-law model, similar to that used by Comastri et al. (1998) in their analysis of a BeppoSAX observation of Ton S180. Fitting with a broken power-law model gave $\chi^2 = 919.1/898$ dof with slopes $\Gamma_1 = 2.98 \pm 0.02$, $\Gamma_2 = 2.22 \pm 0.10$ and a break energy $E_{br} = 2.29 \pm 0.04$ keV. A slightly better fit was obtained using two separate power-laws ($\chi^2 = 910.9/898$ dof) with slopes

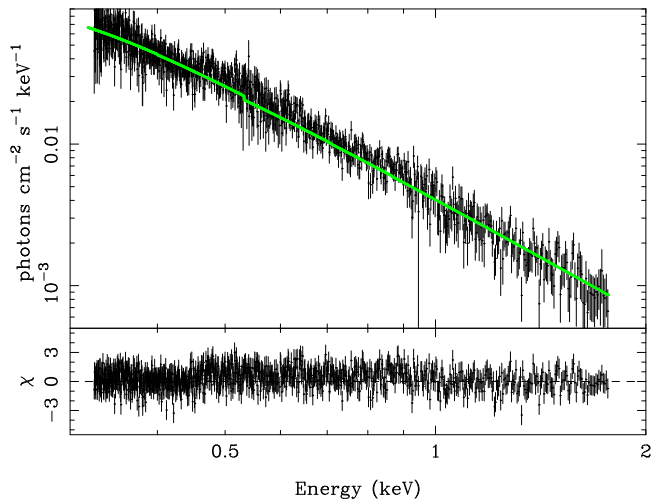


Figure 3. Combined first order RGS spectrum (in “fluxed” units) and best-fitting absorbed power-law model (solid line). The lower panel shows the fit residuals.

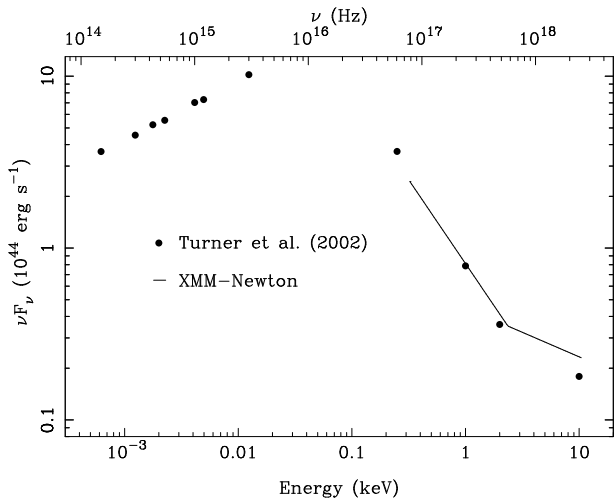


Figure 4. Spectral energy distribution of Ton S180, corrected for Galactic absorption. The solid curve shows the *XMM-Newton* spectrum (using the broken power-law parameterisation discussed in section 3.2.2). The dots show the multiwavelength data from Turner et al. (2002) corrected to match the slightly different cosmology used here.

$\Gamma_1 = 3.11 \pm 0.04$ and $\Gamma_2 = 1.49 \pm 0.15$ (see figure 2). In this model the softer of the two power-laws dominates the spectrum up to ~ 4 keV. The harder power-law is considerably flatter than in the broken power-law parameterisation, due to the addition of the steeper power-law over the whole band, and is perhaps unrealistically flat. These simple fits to the EPIC data, and the RGS results, show that the soft excess has the form of a steep power-law.

Figure 4 places the *XMM-Newton* spectrum in the context of the multiwavelength spectral energy distribution (SED) compiled by Turner et al. (2002). The multiwavelength data were taken approximately one year before the *XMM-Newton* observation, but it is clear that the X-ray spectral form did not change drastically between observations.

3.2.3 Ionised reflection

The possible presence of iron $K\alpha$ emission (section 3.1.1) may indicate significant reflection off the surface of the accretion disc. The reflection spectrum can be strong below ~ 1 keV and could contribute significantly to the soft excess. To test whether the soft excess in Ton S180 could be produced by reprocessing of primary X-rays in the disc reflection model discussed in section 3.1.1 was fitted to the 0.3–10 keV spectrum. The best fitting model obtained for the data above 2.5 keV gave a very poor fit to the broadband data ($\chi^2 = 8351.1/897$ dof). The ionisation state of the reflector means it produces strong O VII recombination emission, not obvious in the data, while the total reflected flux below 2 keV falls far short of the observed soft excess.

Refitting this model to the full-band EPIC data still provided a rather poor fit to the data ($\chi^2 = 1030.4/896$). The best fitting parameters were $\Gamma = 2.58 \pm 0.03$, $R = 1.12^{+0.08}_{-0.12}$, $\log(\xi) = 3.71 \pm 0.06$ and parameters of the LAOR kernel were $r_{\text{in}} < 2.5r_g$ and $i = 46 \pm 8^\circ$ (r_{out} was kept fixed at $400r_g$). In this model the disc surface is highly ionised and produces a smooth excess of emission in the soft band, partly from bremsstrahlung in the irradiated skin of the disc, with relatively weak spectral features. However, this model leaves significant residuals in the fit above 7 keV, where it predicts a strong, ionised iron edge. Thus the low-energy data seemed to require a highly ionised reflector, while the higher-energy spectrum suggested a reflector with much lower ionisation.

Allowing for two reflection components, with different ionisation parameters, improved the fit ($\chi^2 = 964.7/894$ dof). In this fit the continuum slope was $\Gamma = 2.61 \pm 0.02$ incident on reflectors with ionisation parameters $\log(\xi_1) = 4.4 \pm 0.3$ and $\log(\xi_2) = 1.8 \pm 0.1$, the LAOR profile parameters were $r_{\text{in}} < 1.9r_g$ and $i = 41 \pm 6^\circ$. In this model the highly ionised reflector had relative strength $R_1 \approx 0.5$ while the colder reflector was much stronger, with $R_2 \approx 2.4$. Both reflection components contributed to the soft excess emission, but the strong colder reflector improved the fit to the hard X-ray data, although significant residuals still remained above 7 keV. The small inner radius of the LAOR kernel was required in order to smooth sufficiently the recombination features present in the reflection spectra.

3.2.4 Purely thermal soft excess

A power-law plus single blackbody component, to model the soft excess, provided a poor fit to the data ($\chi^2 = 1123.6/898$ dof, see figure 2). Including a second blackbody component significantly improved the fit ($\chi^2 = 912.2/896$ dof), while a power-law plus three blackbodies provided an excellent fit ($\chi^2 = 887.8/894$ dof) with the following parameters: $\Gamma = 2.24 \pm 0.02$, $kT_1 = 33^{+27}_{-9}$ eV, $kT_2 = 103 \pm 5$ eV, $kT_3 = 248 \pm 15$ eV. This multiple blackbody parameterisation is similar to that used to characterise the broadband X-ray spectra of other ultrasoft Seyferts, e.g., RE J1034+396 (Pounds, Done & Osborne, 1995), PKS 0558–504 (O’Brien et al. 2001) and 1H 0419–577 (Page et al. 2002).

However, while this multiple blackbody model did provide an adequate fit to the data, the temperatures and luminosities of these components are at odds with those expected for a simple accretion disc. A standard accretion disc around a $10^7 M_\odot$ black hole should have a peak temperature $\lesssim 40$ eV, much lower than the hottest temperature in the multiple blackbody model. The observed temperatures and luminosities predict sizes of the blackbody emitting regions of $r_{\text{BB}} \sim 3 \times 10^{10}$ cm for the hottest and $r_{\text{BB}} \sim 10^{13}$ cm

for the coolest, which are also difficult to reconcile with a simple accretion disc around a $10^7 M_{\odot}$ black hole ($r_g \sim 1.5 \times 10^{12}$ cm).

Fitting the data with a more realistic thermal accretion disc spectrum, using the DISKPN code (Gierliński et al. 1999), provided a poor fit to the data ($\chi^2 = 1073.7/898$ dof), because the model spectrum is not broad enough, and again it gave an unreasonably high temperature ($kT = 131 \pm 5$ eV). The strong, rapid variability of the soft excess (section 4) also seems incompatible with the expected timescales in a simple accretion disc (see also Boller et al. 1997). These results would seem to reject an origin for the soft excess in terms of (un-modified) thermal emission from an accretion disc. But, as discussed by e.g. Bechtold et al. (1987), Czerny & Elvis (1987) and Ross, Fabian & Mineshige (1992), inverse-Compton scattering in the upper layers of the disc atmosphere should significantly affect the observed high-energy tail of the disc emission. This possibility is discussed below.

3.2.5 Thermal Comptonisation

Inverse-Compton scattering of soft photons in an optically thick medium (i.e., $\tau > 1$; where the diffusion approximation is valid) produces an approximately power-law spectrum at low energies. Thus, as the soft excess in Ton S180 resembles a steep power-law, a Comptonised blackbody component should provide a reasonable fit. The energy index of the Comptonised spectrum is determined by the Compton y -parameter ($y \approx 4\Theta\tau^2$, where $\Theta = kT/m_e c^2$ is the dimensionless electron temperature) according to $\alpha \approx \sqrt{9/4 + 4/y} - 3/2$ (e.g., section 7.7 of Rybicki & Lightman, 1979). This means that it is not possible to solve for both τ and kT from knowledge of the spectral slope alone. Using the double power-law parameterisation of Ton S180 (section 3.2.2) gave a slope of $\alpha = 2.1$ for the soft excess, which corresponds to $y \approx 0.37$ and it is possible to obtain this value, and hence the observed spectral slope, for a range of τ and kT values. A similar situation occurs when considering the optically thin regime, in which case the spectral slope is determined by $\alpha \approx -\ln \tau / \ln(1 + 4\Theta + 16\Theta^2)$. See Zdziarski (1985) and references therein for more details.

The COMPIT code (Titarchuk 1994) was used to model Comptonisation of soft photons in a thermal plasma. A power-law plus Comptonisation component gave a good fit to the data ($\chi^2 = 903.7/896$ dof) with $\Gamma = 1.64 \pm 0.18$ and the soft excess modelled by Comptonisation of a thermal spectrum from a $kT_{\text{bb}} = 60 \pm 7$ eV source. However, for the reasons mentioned above, the temperature and optical depth of the Comptonising plasma are strongly covariant parameters, and thus cannot be constrained simultaneously.

Fitting the spectrum with just two Comptonisation components, similar to the model used by O’Brien et al. (2001) and Page et al. (2002), gave a good fit ($\chi^2 = 891.9/895$ dof). The seed photon temperature was $kT_{\text{bb}} = 56_{-11}^{+6}$ eV, but the parameters of the two plasmas were poorly constrained due to the degeneracy mentioned above. (Similar fits were obtained using the EQPAIR code, discussed below, to model two purely thermal plasmas.) It seems reasonable to associate the source of the soft seed photons with the thermal emission from the inner regions of an optically thick accretion disc. The existence of two discrete Comptonising plasmas is not so easy to explain, especially given that they varied almost identically on short timescales (section 4).

3.2.6 Non-thermal Comptonisation

The double Comptonisation model described above has the two spectrally identified continua (soft and hard power-laws) originating in two distinct thermal Comptonising plasmas. An alternative is that the whole spectrum is produced by a single plasma with a hybrid thermal/non-thermal electron distribution (see Coppi 1999 for a discussion of the physics of such plasmas). Gierliński et al. (1999) modelled the spectrum of the Galactic Black Hole Candidate (GBHC) Cygnus X-1 in its high/soft state in terms of a hybrid plasma. In this model the Cyg X-1 spectrum is comprised of a blackbody from the accretion disc, plus a component due to inverse-Compton scattering of the disc photons in a corona containing both thermal and non-thermal electrons. The non-thermal tail to the electron distribution produces the steep power-law tail of the X-ray spectrum dominating above 10 keV (and observed up to at least ~ 800 keV) and the thermal electrons produce a “soft excess” at a few keV between the non-thermal tail and the accretion disc spectrum. The definite detection of a non-thermal Comptonisation component requires high-energy data, which are not available here, but, as first noted by Pounds et al. (1995), the X-ray spectra of ultrasoft Seyferts do resemble that of Cyg X-1 in its high/soft state. Thus it seems reasonable to test whether a hybrid thermal/non-thermal plasma is a viable model for the X-ray continuum of Ton S180.

The EQPAIR code (Coppi 1992; Gierliński et al. 1999) was used to compute the spectrum formed by Comptonisation of a blackbody photons in a plasma with an hybrid electron distribution. Non-thermal (relativistic) electrons are injected (by some unspecified process) as a power-law in Lorentz factor, γ , into a background thermal plasma, the rate of injection is given by: $\dot{N}_{\text{inj}}(\gamma) \propto \gamma^{-\Gamma_{\text{inj}}}$ (between γ_{min} and γ_{max}). The total optical depth (including that produced by e^{\pm} pairs) and the equilibrium temperature of the thermal component (after accounting for Coulomb heating by non-thermal e^{\pm} and Compton heating/cooling) are computed self-consistently once the initial parameters have been specified. For a detailed discussion of the processes accounted for by this code see Gierliński et al. (1999) and Coppi (1999). The important parameters of the model are the following: the temperature of the input thermal disc spectrum kT_{bb} ; the soft compactness $l_s = L_s \sigma_T / r m_e c^3$, which corresponds to the power supplied by soft seed photons (L_s is the total seed photon luminosity and r is the radius of the emission region); the similarly defined thermal compactness l_{th} , corresponding to the heating supplied to thermal electrons; the non-thermal compactness l_{nth} , which gives the rate of injection of non-thermal electrons; the index of the non-thermal electron injection spectrum Γ_{inj} ; and the optical depth τ_p of the background electron-proton plasma.

With so many parameters (some of which were covariant in the fit) the χ^2 -space contained many local minima. In order to reduce the complexity of the fit some parameters were fixed at physically reasonable values (these are discussed further below). The details of the fitted model parameters will obviously depend on the chosen values for those parameters kept fixed. Thus, while the following fits demonstrate that the EQPAIR model can reproduce the shape of the XMM-Newton spectrum, the exact values of the fitted model parameters should be treated with some caution.

The total compactness $l = l_s + l_h$ (where $l_h = l_{\text{th}} + l_{\text{nth}}$ is the total hard compactness) is not constrained by the XMM-Newton spectra. If the spectrum extends out to $\gtrsim 500$ keV a high compactness will lead to efficient pair production, but the strongest observable consequence of the presence of pairs is an annihilation line at 511 keV. In the absence of this information the soft compactness

was therefore kept fixed at $l_s = 30$ (the lower limit obtained in section 4) and the ratios l_h/l_s and l_{nth}/l_h were used as free parameters in the fitting. Assuming the corona covers the inner disc, the former is related to the ratio of power dissipated in the corona compared to the disc, and the latter gives the fraction of power deposited in the corona that goes into the non-thermal component. The radius of the emitting region was kept fixed at $r = 10^{14}$ cm, this is $\lesssim 70r_g$ for a $\gtrsim 10^7 M_\odot$ black hole, and at the above assumed value of l_s this gives a reasonable soft X-ray luminosity. The temperature of the seed blackbody was fixed at $kT_{bb} = 50$ eV and the minimum and maximum Lorentz factors for the non-thermal injection spectrum were $\gamma_{min} = 1.3$ and $\gamma_{max} = 1000$ (the resulting model spectrum is largely insensitive to the chosen value of γ_{max} when $\Gamma_{inj} > 2$).

The EQPAIR model gave a good fit ($\chi^2 = 892.9/897$ dof) with the following parameters: $l_h/l_s = 0.74 \pm 0.03$, $l_{nth}/l_h = 0.78 \pm 0.02$, $\tau_p = 7.0^{+0.8}_{-1.8}$ and $\Gamma_{inj} = 2.84^{+0.26}_{-0.15}$. Thus there is marginally more power supplied by the seed photons than the coronal electrons, and most of the electron heating is in the form of non-thermal electrons which are injected with a steep spectrum. The soft excess is produced by Compton scattering of the accretion disc spectrum by thermalised electrons, and the emission above a few keV is produced by the non-thermal component. These results are similar to those obtained by Gierliński et al. (1999) for the high/soft state spectrum of Cyg X-1; the significant difference is that in this case the optical depth of the background plasma is much higher than in Cyg X-1. If the optical depth is kept fixed at $\tau_p = 1$ a slightly poorer (but still acceptable) fit is obtained ($\chi^2 = 910.0/898$ dof). Again the soft excess is produced by Compton scattering of seed photons by thermal electrons, and the harder X-ray emission is produced by the non-thermal electrons.

4 TIMING ANALYSIS

This section describes timing analyses of the EPIC data. Results are presented only for the pn data, which have the highest signal-to-noise, but the results were checked against the MOS2 data and the two were found to be entirely consistent. The (1σ) errors on the light curves were calculated using counting statistics.

The topmost panel of figure 5 shows the broad-band (0.2–10 keV) EPIC pn light curve of Ton S180 in 200 s time bins. The light curve is perfectly evenly sampled, uninterrupted and shows a peak-to-peak variation of ~ 50 per cent over the course of the observation. The fastest continuous rise in the light curve occurred at around 2.4×10^4 s, where the flux increased by ~ 30 per cent in 2000 s, corresponding to an increase in luminosity of $\Delta L/\Delta t \approx 3.8 \times 10^{40}$ erg s^{-2} in the 0.3–10 keV band. This was used to estimate the radiative efficiency η of the source, assuming photon diffusion through a spherical mass of accreting matter, following Fabian (1979): $\Delta L/\Delta t \lesssim \eta \cdot 2.1 \times 10^{42}$ erg s^{-2} . (But see also Brandt et al. 1999, for a discussion of the assumptions used in this calculation.) This gave a limit of $\eta \gtrsim 1.8$ per cent. The rapid variability was also used to place a limit on the compactness parameter, following Done & Fabian (1989). Assuming that $r = c\Delta t$ gives $\Delta L/\Delta t \lesssim l \cdot 10^{39}$ erg s^{-2} . For Ton S180 this gave $l \gtrsim 34$.

Figure 5 also shows the pn light curves extracted from five different energy bands in 500 s bins. The light curves all show similar trends, albeit with relatively poor signal-to-noise in the harder bands. The hardness ratios of these light curves were examined as a first test of spectral variability. The ten hardness ratios (six of which are shown in figure 6) from the five light curves were each compared to a constant using a χ^2 test. Four of the ten hardness ra-

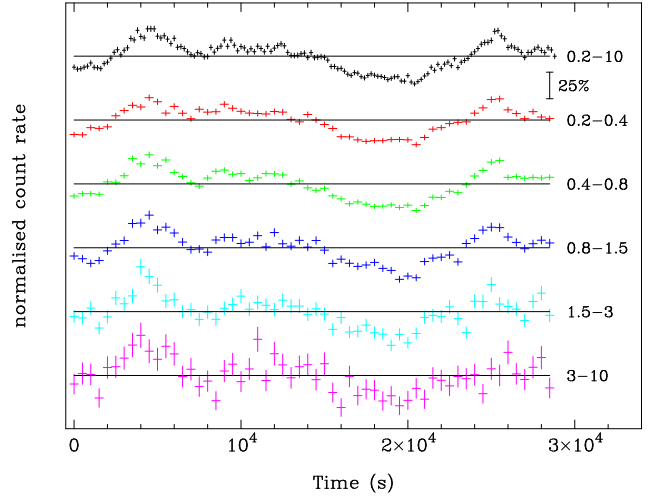


Figure 5. EPIC pn light curves normalised to unit count rate. The topmost panel shows the full-band 0.2–10.0 keV light curve (in 200 s bins) and the lower panels show the light curves from various energy bands (in 500 s bins). The vertical bar indicates the (linear) y -axis scale. The mean count rates for the six light curves (from top to bottom) are as follows: 9.26, 3.26, 3.53, 1.69, 0.56 and 0.22 $ct s^{-1}$.

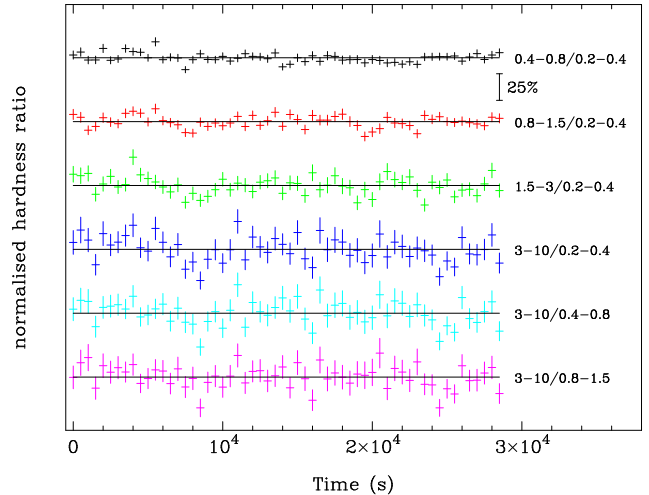


Figure 6. Hardness ratios for various EPIC pn light curves using 500 s time bins.

tios examined were inconsistent with a constant hypothesis at > 99 per cent confidence. These ratios, namely $(0.4 - 0.8)/(0.2 - 0.4)$, $(0.8 - 1.5)/(0.2 - 0.4)$, $(1.5 - 3)/(0.2 - 0.4)$ and $(1.5 - 3)/(0.4 - 0.8)$, are also among the highest signal-to-noise ratios. Using the Spearman rank-order correlation coefficient and the Kendall τ -statistic (see e.g., Press et al. 1992) to test for correlations, none of the hardness ratios was correlated with the broad-band count rate at greater than 90 per cent confidence.

Figure 7 shows a comparison of pn spectra extracted from intervals of high and low flux. These were extracted from only those intervals when the source count rate was above $10 ct s^{-1}$ (high) or below $8.8 ct s^{-1}$ (low). The high and low flux spectra contained $9.6 \times 10^4 ct$ and $8.0 \times 10^4 ct$, respectively. The ratio of high to low flux spectra is consistent with a constant ($\chi^2 = 81.6/84$ dof), again indicating a lack of flux-correlated spectral variability.

The normalised RMS spectrum was calculated in order to quantify the degree of variability in the different energy bands,

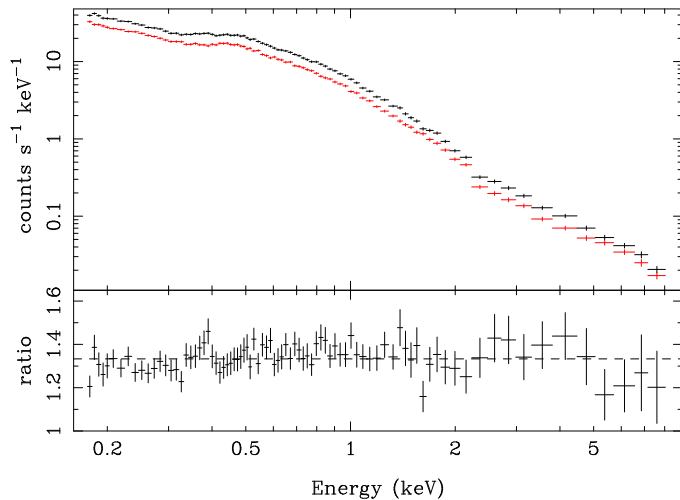


Figure 7. Comparison of high and low flux spectra. The top panel shows the two count spectra taken from high flux (upper crosses, black) and low flux (lower crosses, red) intervals. The bottom panel shows the ratio of high to low flux spectra, which is consistent with a constant (dashed line).

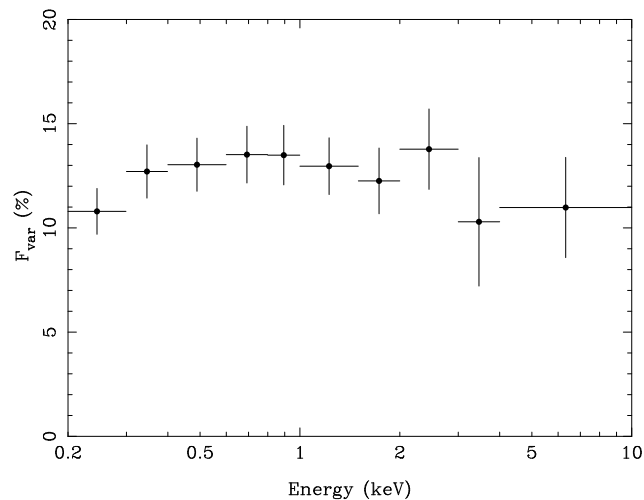


Figure 8. Normalised RMS spectrum based on EPIC pn light curves. The F_{var} values were calculated using 500 s binned data.

again using the 500 s binned light curves. The fractional variability amplitude was measured using the F_{var} statistic (Edelson et al. 2002) which is equal to the square root of the normalised excess variance σ_{XS}^2 (Nandra et al. 1997). The errors were estimated using the formula in Edelson et al. (2002) and should be considered as conservative estimates on the true uncertainties. Figure 8 shows the fractional variability amplitude calculated in ten energy bands, which changes by only 3 per cent over the *XMM-Newton* band-pass. This remarkably flat RMS spectrum contrasts with the situation in many ‘normal’ spectrum Seyfert 1s, which tend to show larger fractional variations at lower energies (e.g. Nandra et al. 1997). Altering the sizes of the time bins or the energy ranges used in the light curves made little difference to the RMS spectrum since most of the variability power is on timescales > 500 s.

Having established that the light curves show similar trends and almost identical amplitudes, the temporal cross-correlation functions (CCFs) were calculated in order to search for leads or lags between different energy bands. The Discrete Correlation Function (DCF) of Edelson & Krolik (1988) was used as an estimator of

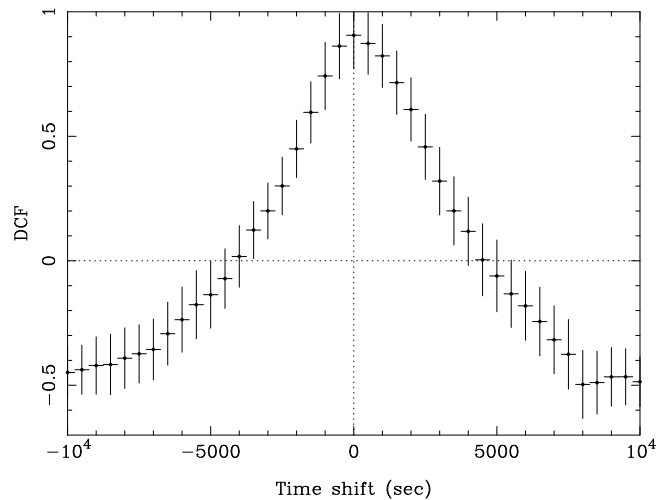


Figure 9. Temporal cross-correlation function for the 0.2–0.3 keV and 0.8–1.0 keV EPIC pn light curves (using 500 s bins), showing a peak at zero lag.

the CCF. The other nine energy bands used in the RMS spectrum were compared to the softest band (0.2–0.3 keV). Of the nine CCFs examined eight peaked at zero-lag (e.g., see figure 9) and the one exception (0.2 – 0.3 keV against 1.5 – 2.0 keV) peaked at a lag of only one time bin (500 s, with the harder band lagging the softer band) which we do not consider to be significant. In all cases the CCF was reasonably symmetric. These results indicate there is no evidence for a lag or lead between the various energy bands to a limit of ± 500 s.

5 DISCUSSION

This paper presents an uninterrupted ~ 30 ksec *XMM-Newton* observation of the ultrasoft, narrow-line Seyfert 1 galaxy Ton S180. The spectrum above 2.5 keV is slightly steeper than the norm for Seyfert 1 galaxies ($\Gamma \approx 2.26$ compared to 1.9) but the iron $K\alpha$ line emission is only poorly constrained. At lower energies the spectrum steepens, seen as a soft excess over the hard X-ray power-law with a featureless, approximately power-law form. The shape of the soft excess is similar to that observed in other objects. For example, Marshall et al. (2002) found the high-resolution soft X-ray spectrum of the ultrasoft Seyfert 1 Mrk 478 (which has a similar X-ray luminosity to Ton S180) was a featureless power-law. PKS 0558–504 also showed a similar soft excess shape (O’Brien et al. 2001). The *Chandra* HETGS observation of the variable, narrow-line Seyfert 1 galaxy NGC 4051 again showed the soft excess to be a rapidly variable continuum component. However, in this lower-luminosity source it showed significant spectral curvature (Collinge et al. 2001).

The observed flux of Ton S180 showed rapid variability, changing by ~ 50 per cent during the observation, but showed only weak spectral variability. This implies that, to first order at least, the curved X-ray spectrum is varying as one component. There are indications that this may be a general result, that Seyferts with steep X-ray spectra show very little spectral variability (at least on short timescales). The *ASCA* monitoring of Ark 564 and Ton S180 showed flat RMS spectra (Turner et al. 2001c; Romano et al. 2001; Edelson et al. 2002), as did the recent *XMM-Newton* observation of 1H 0707–495 (Boller et al. 2002). This lack of short timescale spectral variability is somewhat different from the case in ‘normal’

Seyfert 1s, which tend to show stronger variability at lower energies (e.g., Nandra et al. 1997; Markowitz & Edelson, 2001; Vaughan & Edelson, 2001).

The lack of strong spectral features means that the observed form of the soft excess is consistent with a range of models. The data clearly rule out models based on blends of narrow soft X-ray lines (e.g., Turner et al. 1991), but leave a variety of continuum emission mechanisms as plausible alternatives. Reprocessing of primary X-rays by an ionised accretion disc can produce a strong, smooth excess similar to that observed but has difficulty simultaneously explaining the hard X-ray spectrum (section 3.2.3). The observed lack of spectral variability is also a challenge for this model. The highly correlated, simultaneous variability between 3–10 keV flux (dominated by the primary X-rays) and softer X-ray bands (dominated by the reprocessed emission) requires the reprocessing to produce a near-perfect “reverberation” signature with a delay of $\Delta t < 500$ s (section 4). Assuming a black hole mass of $\gtrsim 10^7 M_{\odot}$ (from the Eddington limit) this places the reprocessor within $\lesssim 10r_g$ of the hard X-ray source.

As first pointed out by Bechtold et al. (1987) the soft excess is too hot to be “bare” thermal emission from the accretion disc. The spectral form is consistent with emission from multiple blackbody components, but the derived temperatures and sizes are inconsistent with those predicted for an accretion disc (unless Ton S180 is highly super-Eddington). Allowing for Doppler and gravitational shifts does not significantly alter this result.

Inverse-Compton scattering of soft photons by thermal electrons provides a more physically satisfying explanation for the broad soft excess (sections 3.2.5 and 3.2.6), in which case the seed photon source is consistent with thermal accretion disc emission. The harder power-law emission extending to 10 keV (and presumably beyond) can also be produced by Comptonisation, either in another purely thermal plasma or by non-thermal electrons in a plasma with a hybrid thermal/non-thermal distribution. Whether this is dominated by thermal or non-thermal electrons is impossible to tell without higher energy data; fits using thermal and hybrid thermal/non-thermal models are comparable in the *XMM-Newton* band, where the predicted spectra both resemble power-laws.

A problem with the models discussed above is that they have difficulty explaining the rapid and energy-independent variability of Ton S180 (section 4). These constraints force the hard and soft X-ray producing regions to be in very close causal contact with one another. If at high accretion rates the disc is puffed-up due to radiation pressure, then it is possible that the separation between the hot corona and the optically thick accretion disc can be negligibly small. In this scenario, some fraction of the accretion energy is dissipated in the surface layers of the disc, producing hot electrons which can Comptonise the soft photons from below. The accretion disc model of Hubeny et al. (2001) demonstrates the formation of a hot upper layer to the accretion disc due to dissipation near the surface (see their figure 10), and simulations of magnetized accretion discs by Miller & Stone (2000) suggest that even higher temperatures may be reached, leading to the formation of a true corona. Simulations of emergent disc spectra accounting for dissipation in the upper atmosphere will be presented elsewhere (Ross et al. in prep.), but early indications suggest that the observed strong, smooth soft excess can be reproduced.

We also note the lack of a significant narrow, neutral iron emission line at 6.4 keV. The formal (90 per cent) upper limit on the equivalent width of such a line is 60 eV, similar to that obtained for 1H 0707–495 by Boller et al. (2002). Again this contrasts with the situation in more normal Seyfert 1s, which tend to show a narrow

6.4 keV emission line from distant, cold material (e.g., Yaqoob, George & Turner, 2002). However, whether this is due to a systematic difference between ultrasoft and normal Seyfert 1s remains to be seen.

ACKNOWLEDGEMENTS

Based on observations obtained with *XMM-Newton*, an ESA science mission with instruments and contributions directly funded by ESA Member States and the USA (NASA). We would like to thank the SOC and SSC teams for making possible the observations and data analysis. We thank Gareth Griffiths for useful discussions about the EPIC calibration and Marek Gierliński for help with the EQPAIR code. We thank the referee, Kim Page, for useful comments. SV acknowledges support from PPARC. DRB acknowledges financial support from the Commonwealth Scholarship and Fellowship Plan and the Natural Sciences and Engineering Research Council of Canada. WNB acknowledges financial support from NASA LTSA grant NAG5-8107 and NASA grant NAG5-9939.

REFERENCES

- Arnaud K. et al. 1985, MNRAS, 217, 105
 Arnaud, K. 1996, in: *Astronomical Data Analysis Software and Systems*, Jacoby, G., Barnes, J., eds., ASP Conf. Series Vol. 101, p17
 Ballantyne, D. R., Iwasawa, K., Fabian, A. C. 2001, MNRAS, 323, 506
 Bechtold, J. Czerny, B., Elvis, M., Fabbiano, G., Green, R. F. 1987, ApJ, 314, 699
 Brandt, W. N., Boller, Th., Fabian, A. C., Ruszkowski, M. 1999, MNRAS, 303, L58
 Brinkmann, W. et al. 2001, A&A, 365, L162
 Boller, Th., Brandt, W. N., Fink H. H. 1996, A&A 305, 53
 Boller, Th. et al. 2002, MNRAS, 329, L1
 Chiang, J., Reynolds, C. S., Blaes, O. M., Nowak, M. A., Murray, N., Madejski, G., Marshall, H. L., Magdziarz, P. 2000, ApJ, 258, 292
 Collinge, M. J., et al. 2001, ApJ, 557, 2
 Comastri, A. et al. 1998, A&A, 333, 31
 Coppi, P. S. 1992, MNRAS, 258, 657
 Coppi, P. S. 1999, in ASP Conf. Ser. 161, “*High Energy Processes in Accreting Black Holes*”, eds. J. Poutanen & R. Svensson (San Francisco: ASP), 375
 Czerny, B., Elvis, M. 1987, ApJ, 312, 305
 den Herder, J. W. et al. 2001, A&A, 365, L7
 Dickey J. M., Lockman F. J. 1990, ARA&A 28, 215
 Done, C., Fabian, A. C. 1989, MNRAS, 240, 81
 Edelson, R., Krolik, J. H. 1988, ApJ, 333, 646
 Edelson, R., Turner, T. J., Pounds, K. A., Vaughan, S., Markowitz, A., Marshall, H., Dobbie, P., Warwick, R. S. 2002, ApJ, 568, 610
 Fabian, A. C. 1979, Proc. R. Soc. London, Ser. A, 366, 449
 Fabian, A. C., Rees, M. J., Stella, L., White, N. E. 1989, MNRAS, 238, 729
 Forster, K., Halpern, J. P. 1996, ApJ, 468, 565
 Gierliński, M., Zdziarski, A. A., Poutanen, J., Coppi, P. S., Ebisawa, K., Johnson, W. N. 1999, MNRAS, 309, 496
 Hubeny, I., Blaes, O., Krolik, J. H., Agol, E. 2001, ApJ, 559, 680
 Jansen, F. et al. 2001, A&A, 365, L1
 Laor, A., Fiore, F., Elvis, M., Wilkes, B. J., McDowell, J. C. 1997, ApJ, 477, 93
 Lawrence, A., Elvis, M., Wilkes, B. J., McHardy, I., Brandt, W. N. 1997, MNRAS, 285, 879
 Leighly, K. 1999a, ApJS, 125, 297
 Leighly, K. 1999b, ApJS, 125, 317
 Marshall, H., Edelson, R., Vaughan, S., Malkan, M. A., O’Brien, P. T., Warwick, R. S. 2002, AJ, submitted

- Mason, K. O. et al. 2001, *A&A*, 365, L36
- Miller, K. A., Stone, J. M. 2000, *ApJ*, 534, 398
- Nandra, K., George, I. M., Mushotzky, R. F., Turner, T. J., Yaqoob, T. 1997, *ApJ*, 476, 70
- O'Brien, P. T. et al. 2001, *A&A*, 365, L122
- Osterbrock, D. E., Pogge, R. 1985, *ApJ* 297, 166
- Page, K. L., Pounds, K. A., Reeves, J. N., O'Brien, P. T. 2002, *MNRAS*, 330, L1
- Pounds, K., Done, C., Osborne, J. 1995, *MNRAS*, 277, L5
- Pravdo, S. H., Nugent, J. J., Nousek, J. A., Jensen, K., Wilson, A. S., Becker, R. H. 1981, *ApJ*, 251, 501
- Press, W. H., Teukolsky, S. A., Vetterling, W. T., Flannery, B. P. 1992, *Numerical Recipes*, Cambridge Univ. Press
- Ross, R. R., Fabian, A. C. 1993, *MNRAS*, 261, 74
- Rybicki, G. B., Lightman, A. P. 1979, *Radiative Processes in Astrophysics*, Wiley: New York
- Strüder, L. et al. 2001, *A&A*, 365, L18
- Titarchuk, L. 1994, *ApJ*, 434, 570
- Turner, M. J. L. et al. 2001a, *A&A*, 365, L27
- Turner, T. J., Weaver, K. A., Mushotzky, R. F., Holt, S. S., Madejski, G. M. 1991, *ApJ*, 381, 85
- Turner, T. J., Pounds, K. A. 1989, *MNRAS*, 240, 833
- Turner, T. J., George, I. M., Nandra, K. 1998, *ApJ*, 508, 648
- Turner, T. J., George, I. M., Nandra, K., Turcan, D. 1999, *ApJ*, 524, 667
- Turner, T. J. et al. 2001b, *ApJ*, 548, L13
- Turner, T. J., Romano, P., George, I. M., Edelson, R., Collier, S. J., Mathur, S., Peterson, B. M. 2001c, *ApJ*, 561, 131
- Turner, T. J., et al. 2002, *ApJ*, 568, 120
- Vaughan, S., Reeves, J., Warwick, R., Edelson, R. 1999, *MNRAS*, 309, 113
- Vaughan, S., Edelson, R., Warwick, R. S., Malkan, M. A., Goad, M. 2001, *MNRAS*, 327, 673
- Vaughan, S., Edelson, R. 2001, *ApJ*, 548, 694
- Yaqoob, T., Goerge, I. M., Turner, T. J. 2002, in *“High Energy Universe at Sharp Focus: Chandra Science”*, eds. S. Vrtilik., E. M. Schlegel, L. Kuhi, (astro-ph/0111428)
- Zdziarski, A. A. 1985, *ApJ*, 289, 514

This paper has been typeset from a \TeX / \LaTeX file prepared by the author.